https://doi.org/10.48048/tis.2024.7907

Impact of Electron-Phonon Coupling on Graphene Intercalation Compounds from Self Energy: Polynomial Models Selection

Pataiy Praiypan[*] and Udomsilp Pinsook

Department of Physics, Faculty of Science, Chulalongkorn University, Bangkok 10330, Thailand

([*]Corresponding author's e-mail: pataiypr@gmail.com)

Received: 2 January 2024, Revised: 7 February 2024, Accepted: 14 February 2024, Published: 30 May 2024

Abstract

In our pursuit of understanding electron-phonon coupling (EPC) and their impact on material properties, we delved deep into the intricate role played by the Eliashberg function in governing electron self-energy. Through meticulous evaluation of tailored polynomial models approximating this function, we unearthed profound insights into how phonon interactions intricately modify electronic energy bands. Employing numerical computations, we meticulously unraveled both the real and imaginary aspects of electron self-energy, crucial in comprehending EPC effects in various materials. Investigating superconductivity within monolayer graphene and its interaction with diverse doping substances, our study led us to identify optimal polynomial models that accurately capture EPC behaviors, offering invaluable implications for predicting critical temperatures in superconducting materials. Expanding the parameters within our models allowed us to anticipate changes in self-energy models for higher-order configurations not explored in this study. Our selection of polynomial spanning degrees from n = 1 to 10 the efficacy of n = 2 (Debye) as the most realistic and accurate model, closely followed by n = 1, albeit occasional deviations observed in specific materials. These discrepancies often stemmed from noise model inaccuracies and parameter approximations. Our comprehensive approach outshone the traditional Kramer-Kronig transform in assessing electron-phonon interactions. Looking ahead, the application of multiple models to the Eliashberg function diagram holds immense promise for enhancing accuracy, despite the challenge of concurrently adjusting multiple input parameters. This integration of numerical modeling with experimental data forms a robust framework, empowering the prediction and fine-tuning of material properties vital for the future fabrication of devices.

Keywords: Conventional superconductor, ARPES, Eliashberg theory, Graphene intercalation compounds

Introduction

Electron Phonon Coupling on electronics structure

Understanding the mechanisms behind electron pairing in superconductors stands as a fundamental pursuit in modern physics. This role belongs to quasiparticle named phonon which is driven by lattice vibrations in enabling electron self-adherence, as expounded by Migdal-Eliashberg (ME) theory. Specifically, the focus lies on how the phonon spectrum influences the phase transition temperature of superconductors, prominently illustrated by the case study of MgB_2. Which has presence of suitable gaps [1] delineated by Fermi surface interactions, underscores the applicability and significance of this theory.

The comprehension of superconductivity not only unveils the governing electronic structures behind distinct properties but also paves the way for advancements in material enhancement. By mitigating electron-photon mode damage and refining surfaces through the modification of graphene, opportunities arise to tailor material properties. This research endeavors to explore the potential of nitroso compounds as promising candidates for further investigation, aiming to deepen our insights into the mechanisms underpinning superconductivity.

The foundation of this study is grounded in the ME theory, which has proven highly successful in elucidating the properties of Conventional Superconductor which related to electron-photon coupling. Moreover, the investigation encompasses the analysis of Angel Resolved Photoelectron Spectroscopy (ARPES), particularly in the context of Electron Phonon Coupling (EPC) within momentum space. We make analysis of the comprehensive measurement of graphene's charge transfer capacity across various additives from Li to Cs [2], without Cs, serves as a crucial dataset contributing significantly to ongoing discussions about the superconducting mechanisms exhibited by these substances.

The main goal of this research is to figure out how electrons and vibrations in materials interact. We'll compare our ideas with existing information to make things clearer. By doing this, we hope to make the graphs we create easier to understand. This helps us see how electronic structure are constructed by phonon affect and how to directly predict superconducting critical temperature from it.

Superconductivity of Graphite Intercalation Compounds

The recent discovery of superconductivity in various Graphite Intercalation Compounds (GICs) has reignited interest in this family of lamellar materials. Notably, the identification of superconductivity in 2 binary GICs, such as YbC_6 [3], CaC_6 [3], LiC_6 [1,4] and NaC_6 [5], boasting remarkably high critical temperatures in both experimental and simulation, brought a significant shift in focus. In particular, GICs containing calcium display critical temperatures approximately one order of magnitude higher than those previously experimental studied [6]. However, it has been argued from simulation [4] that sodium on GICs can has more.

Despite considerable efforts, superconductivity remains elusive in monolayer graphene, despite its impressive electronic properties. Theoretical suggestions proposed enhancing EPC by decorating graphene with an alkali adatom superlattice to potentially induce superconductivity. Experimental evidence supports the enhancement of EPC due to adatom decoration, but actual superconductivity has not been observed. Through Angle Resolved Photoelectron Spectroscopy (ARPES), our research demonstrates that depositing lithium on graphene at low temperatures significantly alters the phonon density of states, resulting in an increased EPC.

Their focus is on finding a high EPC system, specifically their exploring of graphene's π^* bands for sustaining superconductivity [2]. Using the ARPES technique, they assess the electronic band structure and extract the Eliashberg functions of graphene doped with Cs, K, Na, Rb, Li and Ca. The outcomes reveal a distinct low-energy peak influenced by the dopant atom, suggesting a connection to a dopant-related vibration. Particularly, the significant charge transfer from Ca, along with its phonon, significantly contributes to EPC, potentially enabling superconductivity at 1.5 K in Ca-doped graphene.

Angle resolved photoelectron spectroscopy

ARPES experiments [7] unveil the clear manifestation of EPC through abrupt alterations in electronic band dispersions and linewidths, directly linked to shifts in the real and imaginary components of the electronic self-energy (Σ', Σ''). The analysis of ARPES cuts aligned with previous measurements highlights substantial changes in the Fermi surface of graphene-based GICs, primarily driven by factors such as ionization and distorted electronic bandlines, extensively investigated [2]. The presence of impurities' free electrons potentially pairing with in-plane and contamination-induced phonons significantly influences structural connections. Lower phonon energy holds a critical role in shaping these new connections, owing to the direct relationship between EPC and reciprocal phonon energy, leading to pronounced shifts in orbital overlap due to greater amplitudes in low-energy vibrations. Despite detection constraints, indications of potential C_{xy} modes persist. These findings not only confirm theoretical predictions but also validate the existence of modes on specific bands through observed Σ' and Σ'' widths and peak-step correspondences, solidifying the credibility of identified kinks.

Furthermore, their study highlights an overlap of C_z mode features on both π^* and IL bands, indicating shared coupling between these bands by common C_z modes. This agreement between experimental data and theoretical predictions strengthens the understanding of EPC mechanisms in these materials. They observed kinks in band dispersions, mirrored in Σ' and Σ'' with finite widths, underscore the role of specific phonon modes in influencing electronic properties. Despite technical limitations, these findings provide crucial insights into the nature and impact of electron-phonon interactions on band structures, offering a comprehensive understanding of these coupling mechanisms within the context of the studied materials.

The core of their study lies in conducting high-resolution ARPES measurements along the kink region within the ΓK and KM high-symmetry directions [7]. These meticulously acquired data serve as the foundation for extracting crucial parameters like the electron self-energy Σ', employing a method detailed in our analysis. The resulting Σ' and Σ'', rigorously Kramers-Kronig consistent, are prominently featured in **Figure 1**, alongside the Eliashberg function, offering a comprehensive view of the system's behavior. Central to our findings are the dopant-specific Eliashberg functions, which emerge as the linchpin in deciphering EPC and unraveling the intricacies of superconductivity in doped graphene. A precise modeling of Σ reveals the necessity for 2 (3) Lorentzians [8], remarkably mirroring experimental observations in both ΓK and KM directions. Notably, in KM, the distinct low-energy peak, prominently associated with Ca doping, is visibly represented as a shoulder in Σ' and an additional step in Σ'', accentuating the dopant-dependent features within the superconducting behavior.

This excerpt delves into the profound impact of EPC on the dispersion and lifetime of electronic states within a material. It underscores the pivotal role of surface states in elucidating the bosonic spectroscopic signature arising from the EPC. The discussion navigates through the alteration in dispersion and lifetime of electronic states, highlighting the emergence of a complex self-energy and its components that reshape the behavior of these states.

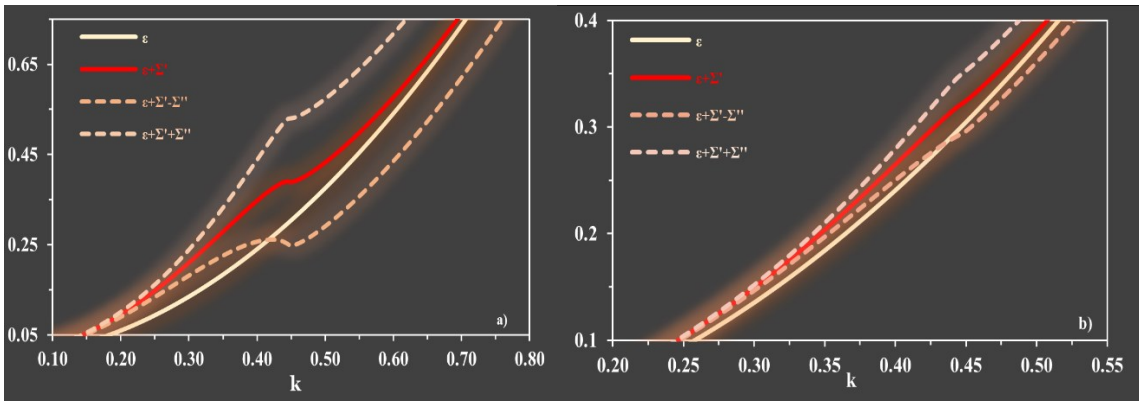

Figure 1 specifically ARPES cuts of the model a) n = 1 and b) n = 2 with demonstrate quite high electron phonon interaction, ω_0 = 0.3 eV, C = 1 along arbitrary path. 'k' represents wavefunction's momentum magnitude in unit of nm^{-1}. Vertical values in unit of eV. Each energy defined in methods (Eqs. (1) - (3), respectively)

Figure 1 illustrates kinks of electronics bareband with adding EPC, when change the interaction, we expect that every single coupling strength should be cause of deviate the energy curve. No matter what direction of k-space be considered, all ARPES cuts should be similar in the same substance with the same physical conditions. And we need to crop for seeing more details when adding more degrees, which means lower EPC. The order of the model (n) will be defined later, as indicated by equation (5).

Materials and methods

The Eliashberg function is the key factor governing both parts of the complex electron self-energy, intricately dictating the dispersion modification and lifetime emergence in electronic states. This function encapsulates the comprehensive description of how the electron-phonon interaction influences the behavior of these states within a material.

In this study, we will demonstrate that the twisting of the energy lines, caused by ARPES as in **introduction** section, affects the Eliashberg function, ultimately influencing the energy band structure. This energy band structure can be clearly observed through ARPES. The samples [7] we examined are from charge density waves (CDW), allowing us to define the energy function in ARPES, which states the rate of scattering of electrons-phonons [8]. This function is referred to as electron self-energy. As it involves the scattering of electron-phonon, we may express it in the form of EPC.

The interaction with phonons results in the renormalization of electronic energy bands, a phenomenon revealed through the real part of the self-energy [9]. This component enables the assessment of the bared band dispersion, illustrating the influence of phonon interaction on electronic states.

$$\Sigma' = -\int_0^\infty d\omega\, \alpha^2F(\omega)\ln\left|\frac{\omega+\varepsilon}{\omega-\varepsilon}\right| \quad (1)$$

$$\Sigma'' = -\pi\int_0^\epsilon d\omega\, \alpha^2F(\omega) \quad (2)$$

$$E(\mathbf{k}) = \varepsilon(\mathbf{k}) + \Sigma'(\mathbf{k}) \quad (3)$$

When $E(\boldsymbol{k})$ is renormalized band dispersion, $\varepsilon(\boldsymbol{k})$ is bareband dispersion without EPC, Σ' and Σ'' are real and imaginary parts of electrons self energy at absolute zero temperature, respectively. $\alpha^2F(\omega)$ is the State-dependent Eliashberg function, which is defined by:

$$\alpha^2F(\omega) = \sum_{\mathbf{k},\mathbf{q}}\left|g_{\mathbf{k},\mathbf{q}}\right|^2\delta\left(\epsilon_{\mathbf{k}} - \epsilon_{\mathbf{k}\pm\mathbf{q}}\right)\delta\left(\omega - \omega_{\mathbf{q}}\right). \quad (4)$$

The complexity of evaluating Eq. (4) necessitates the adoption of suitable model(s) to characterize the Eliashberg function's behavior. Employing these chosen models allows for the formulation of polynomial representations to approximate the intricacies outlined in Eq. (4). This approach enables a more manageable analysis of the Eliashberg function curve within the context of the defined polynomial models.

$$\alpha^2F(\omega) = \begin{cases} C\omega^n ; 0 \le \omega \le \omega_0 \\ 0 \quad ; \text{elsewhere} \end{cases} \tag{5}$$

When C is real number constant, n is an integer that can varied from 0 to 10 (when n = 0 it is simply the rectangle model [10]). ω_0 represents cutoff frequency for each model. Then, we use each model in Eq. (5) calculate Eq. (1) for finding self energy using trapezoidal integration.

The study [2] investigates inducing superconductivity in monolayer graphene via CaC_6, finding a superconducting gap in the graphene-derived band and significant electron-phonon interaction between graphene and the interlayer band. It suggests that surface adatoms creating an interlayer band could enable superconductivity in monolayer graphene, emphasizing ARPES's role in measuring band properties crucial for future graphene-based device fabrication. Their data lead us to from initial Σ" function and from Eq. (2) transform it as derivatives to,

$$\alpha^2F(\omega) = -\frac{1}{\pi}\frac{\partial\Sigma''}{\partial\epsilon}\Big|_{\epsilon=\omega} \tag{6}$$

Tracing the experimental data in [2] for doping substances: Li, Ca, Na, Rb and K (excluding Cs due to its unclear evidence of possessing a nonzero critical temperature when calculated) revealed the impact of tiny electron-phonon interactions. Eq. (6), easily solvable numerically, involves using the Newton Forward first divided difference to compile derivatives. By leveraging the calculated derivatives of the imaginary part, we determine the real part by substituting it into Eq. (1). The integration computation employs the trapezoidal rule. This approach includes comparing the peaks of the real part and the imaginary part, serving as a tool to select a model from **Table 1**, as shown in Eq. (7).

$$r_1 = \pi\frac{\Sigma'_{max}}{\Sigma''_{max}} \tag{7}$$

When r_1 represents a choosing parameter, for example if the substance exhibits $\Sigma'_{max} = \Sigma''_{max}$, we have $r_1 = \pi$. Subsequently, referring to **Table 1**, we select the 3rd model. This leads us to hypothesize that the most suitable model should entail $n \le 3$. We applied this method for substances from [2]. Fitting the experimental implied data and the modeled data $\alpha^2F(\omega)$ by recalculating the Real part in Eq. (1). By adjusting input from Eq. (5) to align with the curve outputs in both low bare electron energy and high bare electron energy zones, respectively.

Calculated $\alpha^2F(\omega)$ from Eq. (6) may have some experimental noise. We fixed it via using reconstruct parameter r_2, which is defined by,

$$r_2 = \frac{\Sigma''_{tr,max}}{\Sigma''_{calc,max}} \tag{8}$$

While $\Sigma''_{tr,max}$ represents traced data of self energy imaginary part from [2], $\Sigma''_{calc,max}$ refers to the calculated counterpart obtained from Eq. (6) and subsequently integrated back into Eq. (2). In an ideal scenario, r_2 should equal to 1. After taking the value of r_2, we multiply it back into the EPC function, ensuring preservation of the interaction despite distortion from carving noise. Using the final result of $\alpha^2F(\omega)$, we calculated the McMillan critical temperature (Eqs. (9) - (11)), The final results are shown in **Table 2**.

$$T_c = \frac{\omega_{ln}}{1.2}\exp\left\{-\frac{1.04(1+\lambda)}{\lambda - \mu^*(1+0.62\lambda)}\right\} \tag{9}$$

$$\lambda = 2\int_0^\infty \frac{\alpha^2F(\omega)}{\omega}\,d\omega \tag{10}$$

$$\omega_{ln} = exp\left\{\frac{2}{\lambda}\int_0^\infty \frac{\alpha^2F(\omega)}{\omega} ln\omega\, d\omega\right\} \tag{11}$$

When T_c is critical temperature, λ is average (Isotropic) EPC strength. ω_{ln} is simply log-averaging method for phonon frequency.

Results and discussion

The application of polynomial models, detailed in Eq. (5), enabled the computation of real self-energy components in Eq. (1). Employing the trapezoidal rule with specific widths ($\Delta\omega = 0.002$ eV, $\Delta\epsilon = 0.008$ eV) allowed for the visualization depicted in **Figure 1**, showcasing an illustrative example with n = 1 (right triangle model). Increasing the cutoff frequency (ω_0) induces a rise in the self-energy peak and amplifies the full width half maximum, while augmenting the polynomial coefficient (C) corresponds to a heightened rate of growth for each degree. These findings suggest that an increased area correlates with intensified electron confinement due to enhanced phonon interaction. Examining the n = 2 model, known as Debye's model, underscores the significance of elevating the cutoff frequency and interaction coefficient for accurate representation, frequently employed in Eliashberg functions and phonon density of states [11]. However, careful consideration of the self-energy factor is essential to ensure precise reference to the original data when utilizing this or similar models.

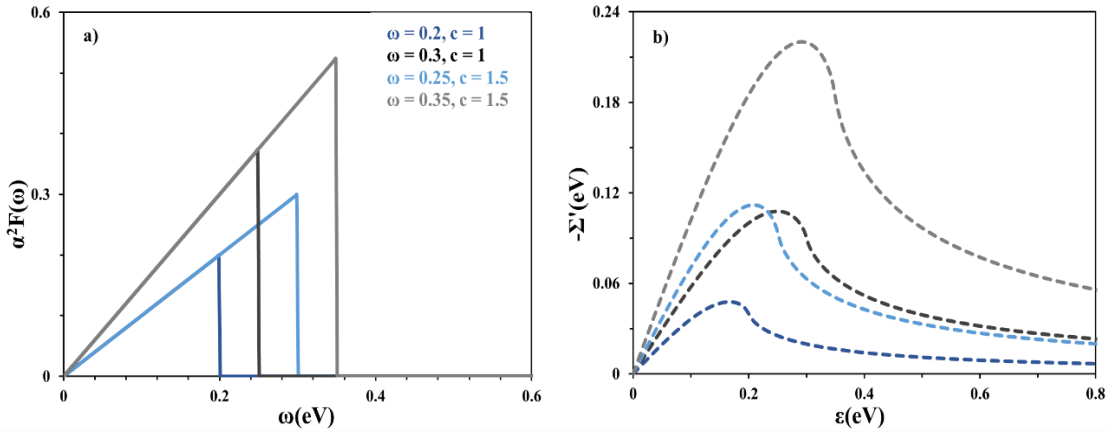

Figure 2 a) Eliashberg functions of n = 1 (solid lines) varying cutoff (ω_0) and slope (C) and **b)** their Real self energies (dash lines with corresponding color). Note that the self energies have the same unit as frequencies and electron energies.

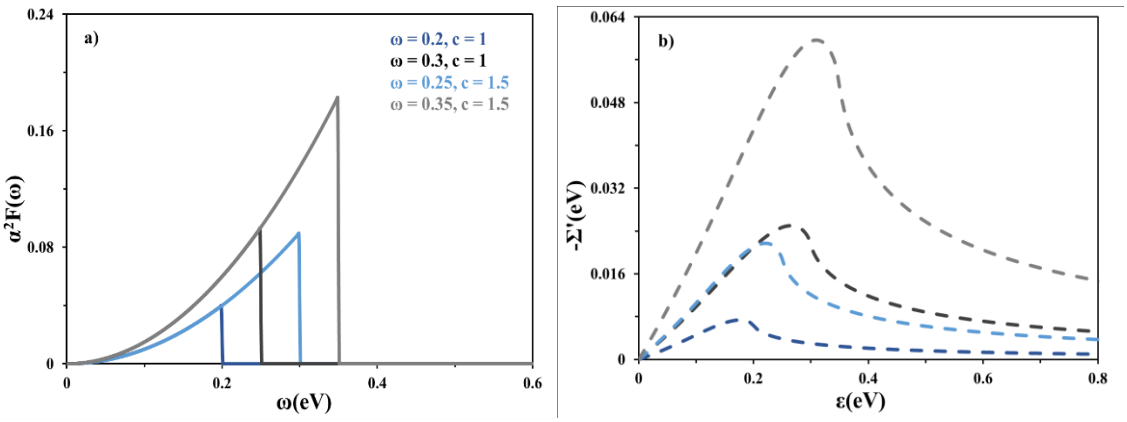

Figure 3 a) Eliashberg functions of n = 2 (solid lines) varying cutoff (ω_0) and slope (C) and **b)** their Real self energies (dash lines with corresponding color). Note that the self energies have the same unit as frequencies and electron energies.

In observing the relationship between the real part of the peak of self-energy concerning the aforementioned variations, a noticeable progressive increase becomes evident. The resultant graphical representation showcases a linear trend akin to that depicted in **Figure 2**. Our approach involves employing higher orders beyond solely n = 1, leading to the identification of 10 distinct straight lines, each

characterized by varying slopes. The gradients associated with each model illustrated in **Figure 2** have been systematically gathered in **Table 1**. Leveraging this data set, we construct the relationship depicted in **Figure 4**, establishing criteria expressed as intervals delineating the correlation between the peak of each model (ranging from n = 1 to n = 10) and the gradient pertaining to each line within **Figure 2**.

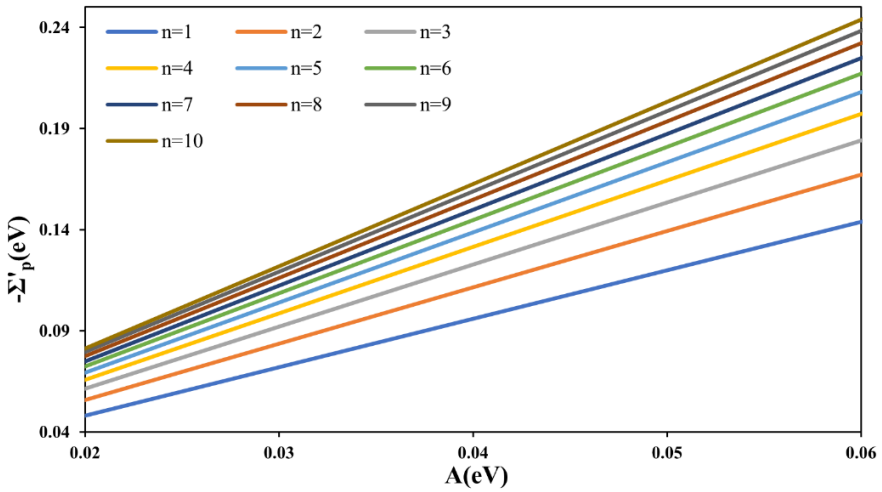

Figure 4 Peak of real self energies (vertical) vs areas (horizontal) of the Spectral functions (represented by polynomial model) varied from n = 1 through 10.

The establishment of the correlation between the peaks of self-energy, as delineated in **Figure 4**, is elucidated through a discernible linear trend characterized by an escalating gradient. This observed relationship is concomitantly corroborated by the findings illustrated in **Figures 2** and **3**, wherein a progression from a model power of 1 to 2, under consistent coefficients and cutoff values (e.g. c = 1, ω_0 = 0.2), manifests an augmentation in the model's power (n). The ensuing implication is a proportional elevation in the corresponding peak magnitude with respect to area of a corresponding model. This discernible trend prompts the inference that an incremental augmentation in the model power, represented by the parameter 'n', results in a concomitant augmentation in peak amplitude. Additionally, an extrapolation is posited, asserting that alterations in the model's power give rise to consequential variations in other facets of self-energy. Furthermore, an exhaustive compilation of the relationships between 'n' and the associated gradients is undertaken. Subsequently, a logarithmic curve (displayed in **Figure 5**) fitting is applied to discern patterns, facilitating the identification of optimal time intervals for parameter selection.

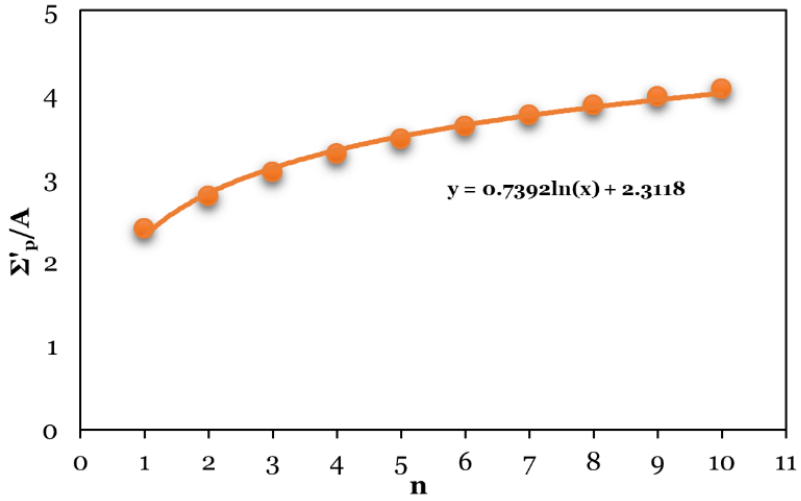

Figure 5 Collect all slope values from the lines in Figure 4 and plot them together to form a log-fit curve, as shown in the graph. Using the equation of this log-fit curve, calculate the error bars for each n^{th} degree (±0.5 from the base value) to create a suitable range, as presented in **Table 1**.

Table 1 Polynomial's model of nth degree and their criteria's interval of factor r_1.

n	Σ'_p/Area	r_1(interval)
0	-	1.7994 or less
1	2.3966	1.7995-2.6115
2	2.7873	2.6116-2.9891
3	3.0678	2.9892-3.2378
4	3.2880	3.2379-3.4236
5	3.4681	3.4237-3.5719
6	3.6200	3.5720-3.6954
7	3.7484	3.6955-3.8012
8	3.8691	3.8013-3.8937
9	3.9720	3.8938-3.9759
10	4.0662	3.9760-4.0499

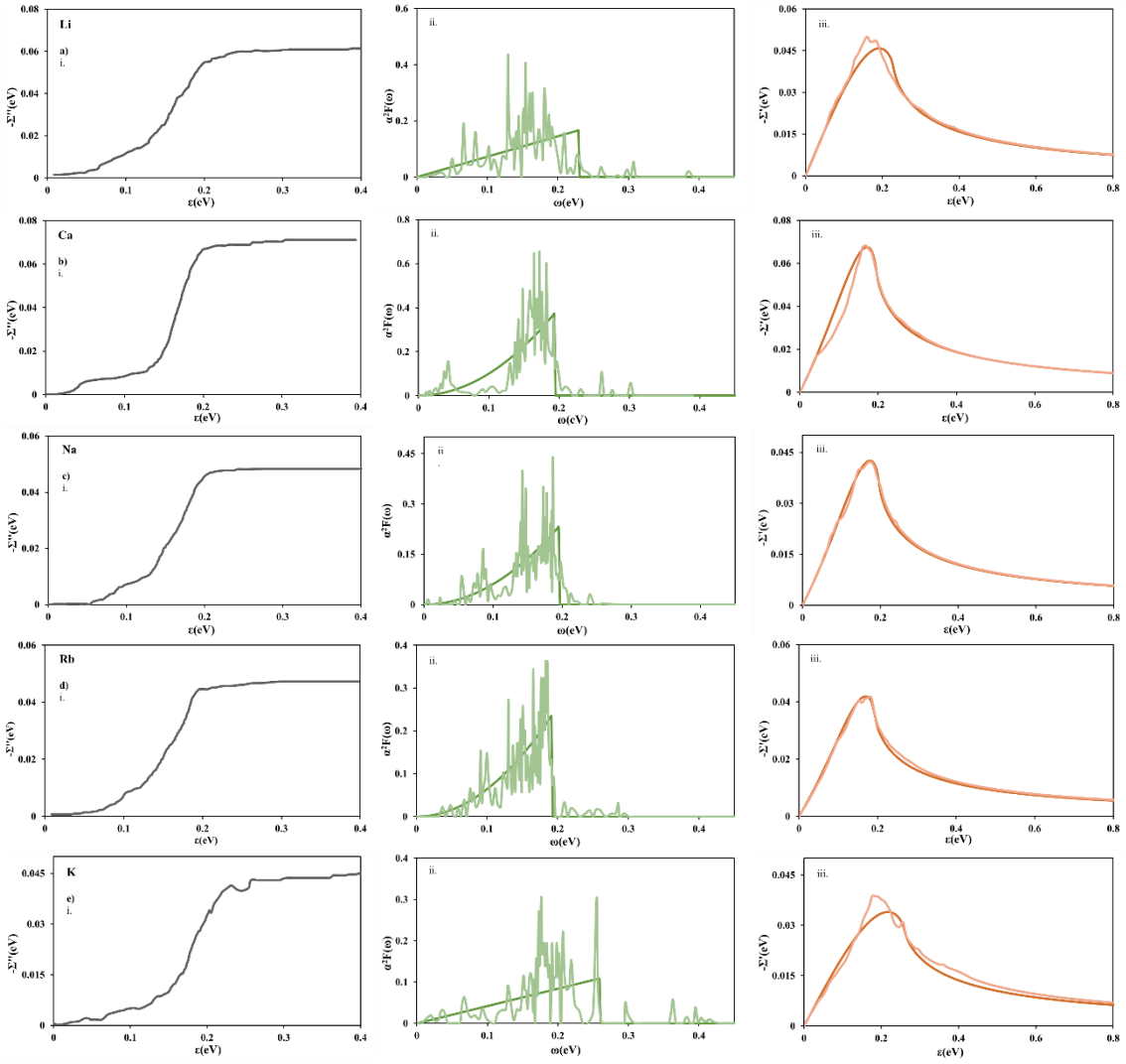

Figure 6 i) and **iii)** Self energies and **ii)** Eliashberg functions of all 5 dopants on C_6 by starting from the imaginary parts of self energy from the experiments traced from [2] (solid lines) with Eq. (6) leading to the graph. The Eliashberg function (wavy, light lines) then creates the electron energy domain to calculate the real part (wavy, light lines) with Eq. (1). In the same graphs, compare with fitting our data using a polynomial model (smooth, dark lines) as shown in degree (n) as in **Table 2**. Arrange the parameter values as follows: Ca ω_0 = 0.195 eV and c = 10, Li ω_0 = 0.23 eV and c = 0.725, Na ω_0 = 0.197 eV and c = 6.1, Rb ω_0 = 0.193 eV and c = 0.641, K ω_0 = 0.261 eV and c = 0.42.

The findings derived from Eq. (6) and subsequently refined with r_2 from the referenced 5 samples in [2] form the basis of our analysis. Our approach involves determining the precise real part value and employing r_2 to select the most suitable model. By putting the data in **Table 1**, we aim to correct the real part curves for both minimal and substantial bare energies. The depiction of these outcomes in **Figure 6**, referenced to **Figure 6(ii)**. for each substance, dark lines represent the refined values from **Figure 6(iii)**. This alignment facilitates the convergence of average EPC and average frequency. It is imperative that these results maintain accuracy in their estimation of the critical temperature.

The calculation results for finding Critical temperature have been collected in **Table 2**. From this table implies that the more fitted graphs the more close of final output (Critical temperature). And Debye model (n = 2) can be considered as the best fitted when we pick some single polynomial model. However, we can make more assumption that the peak of both parts of self energy are relate to each other because they are correlated by electron phonon interaction throughout bareband energy, as illustrated in **Figure 1**.

Figure 6 illustrates all materials we used. Characteristics in terms of fixed properties observed in real energy, notably highlighting Na and Rb as exemplars of stability. The corresponding critical temperature (T_c) values in **Table 2** stand at 25.5 mK and 28.9 mK, respectively. However, Ca dopant exhibits a departure from this pattern, displaying light line distortion and gives a specially highest T_c of 3.97 K which is quite lower from [3], indicating substantial deviation within this model. This distinction positions calcium as an outlier compared to other materials, ranking 2nd in reliability only to Li (with 1.1953 K) and K (with 4.9 mK). The deviations of all dopants arises from non-linear peak shapes, differing from the anticipated straight peak patterns observed in other substances.

Table 2 (left to right) fitting polynomial nth order, corresponding fitting factors with respect to data from experiment, Critical temperatures of each doping substance.

Dopant	n	r_1	r_2	T_c[K]
Ca	2	2.9426	0.9441	3.9733
Li	1	2.5757	0.9199	1.1953
Na	2	2.7564	0.9222	0.0255
Rb	2	2.8052	0.9927	0.0289
K	1	2.5021	0.8504	0.0049

Conclusions

By increasing the cutoff value and coefficient of each model, thus implicitly increasing EPC, we can accurately predict that for other models (n = 3 and above) not applied in this task, the self-energy model and its maximum value will follow the changes in these input parameters. The relationship between the maximum value and space is clearly demonstrated in **Table 2**. Furthermore, we have found that the most realistic and accurate model we adopted is n = 2, followed by n = 1. However, for n = 1 in Li and K, it is rarely an even point, whereas other shapes may be even points. This discrepancy might be attributed to inaccuracies in the noise model drawing and Newton's divide difference approximation (We use $\Delta\varepsilon$ in meV order of magnitude. While energy's horizontal scale is 0.1 eV). We believe our results are more accurate than those obtained using the Kramer-Kronig transform [2].

Incidentally, the successful of the Debye model (n = 2) has been applied to model both the Eliashberg function [12] and the Phonon density of states [11]. However, it is crucial to consider the crystal structure and electronic configuration of the substance used [13], as emphasized in subsequent studies. We anticipate that our other polynomial functions (when applied at different n values) will also find practical application.

The next step in this task involves assembling each model and applying it to the Eliashberg function diagram, which could potentially provide higher accuracy than before. Given the different application methods, it is essential to bear in mind that this might yield more than 2 input parameters, which could prove quite challenging to adjust.

Acknowledgements

We acknowledge from Jakkapat Siyangnok, Muneeb Ul Hassan for several great discussions and advisements and the supporting computing infrastructure provided by NSTDA, CU, CUAASC, NSRF via PMUB [B05F650021, B37G660013] (Thailand).

References

[1] BM Ludbrook. 2014, Electron-phonon mediated superconductivity probed by ARPES: From MgB2 to lithium-decorated graphene. Master Thesis. University of British Colombia, British Colombia, Canada.

[2] AV Fedorov, NI Verbitskiy, D Haberer, C Struzzi, L Petaccia, D Usachov, OY Vilkov, DV Vyalikh, J Fink, M Knupfer, B Büchner and A Grüneis. Observation of a universal donor-dependent vibrational mode in graphene. *Nat. Comm.* 2014; **5**, 3257.

[3] TE Weller, M Ellerby, SS Saxena, RP Smith and NT Skipper. Superconductivity in the intercalated graphite compounds C_6Yb and C_6Ca. *Nat. Phys*. 2005; **1**, 39-41.

[4] H Zhang, C Bao, Ml Schuler, S Zhou, Q Li, L Luo, W Yao, Z Wang, TP Devereaux and S Zhou. Self-energy dynamics and the mode-specific phonon threshold effect in Kekule-ordered graphene. *Natl. Sci. Rev*. 2022; **9**, nwab175.

[5] CM Hao, X Li, AR Oganov, J Hou, S Ding, Y Ge, L Wang, X Dong, HT Wang, G Yang, XF Zhou and Y Tian. Superconductivity in graphite intercalation compounds with sodium. *Phys. Rev. B* 2023; **108**, 214507.

[6] N Emery, C Hérold, JF Marêché and P Lagrange. Synthesis and superconducting properties of CaC6. *Sci. Tech. Adv. Mater*. 2008; **9**, 44102.

[7] SL Yang, JA Sobota, CA Howard, CJ Pickard, M Hashimoto, DH Lu, SK Mo, PS Kirchmann and ZX Shen. Superconducting graphene sheets in CaC_6 enabled by phonon-mediated interband interactions. *Nat. Comm*. 2014; **5**, 3493.

[8] F Marsiglio. Phonon self-energy effects in Migdal-Eliashberg theory, Available at: https://arxiv.org/abs/2101.12084, accessed October 2026.

[9] P Hofmann, IY Sklyadneva, EDL Rienks and EV Chulkov. Electron-phonon coupling at surfaces and interfaces. *New J. Phys*. 2009; **11**, 125005.

[10] U Pinsook. In search for near-room-temperature superconducting critical temperature of metal superhydrides under high pressure: A review. *J. Met. Mater. Miner.* 2020; **30**, 31-41.

[11] AM Brown, R Sundararaman. Ab *initio* phonon coupling and optical response of hot electrons in plasmonic metals. *Phys. Rev. B* 2016; **94**, 75120.

[12] A Nojima, K Yamashita and B Hellsing. Model Eliashberg functions for surface states. *Appl. Surf. Sci*. 2008; **254**, 7938-41.

[13] F Schrodi, A Aperis and PM Oppeneer. Influence of phonon renormalization in eliashberg theory for superconductivity in two- and three-dimensional systems. *Phys. Rev. B* 2021; **103**, 64511.

[14] M Gao, ZY Lu and T Xiang. Prediction of phonon-mediated high-temperature superconductivity in Li3B4C2. *Phys. Rev. B* 2015; **91**, 45132.

[15] A Bostwick, T Ohta, T Seyller, K Horn and E Rotenberg. Experimental determination of the spectral function of graphene, Available at: https://arxiv.org/abs/cond-mat/0609660, accessed October 2026.